# Effects of the Nature and Concentration of Salt on the Interaction of the HIV-1 Nucleocapsid Protein with SL3 RNA[§]

**Shreyas S. Athavale**[**], **Wei Ouyang**, **Mark P. McPike**, **Bruce S. Hudson**, and **Philip N. Borer**
Department of Chemistry, Syracuse University, Syracuse, NY 13244

Shreyas S. Athavale: shreyas.athavale@biology.gatech.edu; Wei Ouyang: wouyang@syr.edu; Mark P. McPike: mpmcpike@syr.edu; Bruce S. Hudson: bshudson@syr.edu; Philip N. Borer: pnborer@syr.edu

## Abstract

The mature nucleocapsid protein of HIV-1, NCp7, and the NC-domains in gag-precursors are attractive targets for anti-AIDS drug discovery. The stability of the 1:1 complex of NCp7 with a 20mer mimic of stem-loop 3 RNA (SL3, also called psi-RNA, in the packaging domain of genomic RNA) is strongly affected by changes in ionic strength. NC-domains recognize and specifically package genomic HIV-1 RNA, while electrostatic attractions and high concentrations of protein and RNA drive NCp7 to completely coat the RNA in the mature virion. The specific interactions from NCp7-binding to loop bases of SL3 produce 1:1 complexes in solutions that have [NaCl] at or above 0.2 M, while the electrostatic interactions can dominate at and below 0.15 M NaCl, leading to complexes that have mainly 1:2 RNA:protein. Persistent, non-equilibrium mixtures of 1:1 and protein-excess complexes can exist at these lower salt concentrations, where the distribution of complexes depends on the order of addition of RNA and protein. Adding salt causes rapid rearrangement of metastable multi-protein complexes to 1:1. The stability of complexes is also affected by the nature of the added salt, with 0.018 M $MgCl_2$ and 0.200 M added NaCl producing the same $K_d$ ($21 \pm 2$ nM); acetate ion stabilizes the 1:1 complex by more than a factor of two compared to the same concentration of chloride ion. Maintaining a salt concentration of 0.2 M NaCl or 18 mM $MgCl_2$ is sufficient for experiments to distinguish drug candidates that disrupt the specific SL3-NCp7 interactions in the 1:1 complex.

## Keywords

RNA; HIV-1; nucleocapsid protein; fluorescence

The nucleocapsid protein of HIV-1 is an attractive anti-AIDS drug target. In addition to its role in packaging the RNA (1–4), it has chaperoning functions (5–6), helps refold the RNA dimer (7–9), and anneals the primer tRNA onto genomic RNA for reverse transcription (10–11). It also interacts with viral proteins including reverse transcriptase (12–13), and the accessory protein, Vpr, to play a role in stable integration of the proviral DNA in the chromosomes of infected cells (14). Drugs targeted at NC have the potential to interfere with critical functions at many stages of the viral infection cycle (6,9,11,15–18).

In retroviruses similar to HIV-1 about 2,000 polyprotein precursors (gag and gag-pol) assemble at the inner membrane of the forming virion (19–21). Each of these proteins contains a nucleocapsid domain that is required for packaging genomic RNA into new virus particles. The 55 kD gag precursor polyprotein is later processed by the viral protease to structural proteins, including the mature NCp7 (20). NC-domains within gag precursors bind to the RNA with several RNA-NC interactions responsible for full discrimination of genomic from non-genomic RNA (22–27). Both sequence-specific and non-sequence-specific contacts contribute to the free energy of binding (22–30).

The NC domain of gag-precursor proteins and the mature NCp7 protein bind with high affinity to stem-loop 3 (SL3, also called the packaging or Ψ-loop) located at nt 312–325 in the 5′-untranslated region of genomic RNA (see Figure 1). Sequence-specific interactions are important in defining the structure of the SL3-NCp7 packaging complex (31). G318 stacks on W37, leading to nearly full quenching of the tryptophan fluorescence and straightforward analysis of binding isotherms (27,31–35). The dissociation constant was reported as $28 \pm 6$ nM in 0.2 M NaCl for the complex (32), revised here to $K_d = 21 \pm 2$ nM. Non-sequence-specific interactions, which are largely electrostatic, also contribute to affinity because of the high charges of the fully ionized species: −19 for the SL3 20mer and +9 for NCp7 (pNL4-3 strain; see legend to Figure 1).

The non-sequence-specific interaction dominates in the mature virion where there is roughly one NCp7 per seven to ten nucleotides. This interaction allows the RNA and protein to collapse to a chromatin-like density. The protein concentration is >10 mM in the mature nucleocapsid, so more than 95% of RNA 10mer segments would be bound by NCp7 even for sequences with a thousand-fold lower affinity than SL3.

It has been appreciated for more than 10 years that complexes of ~20mer oligonucleotides with NCp7 can have stoichiometries other than 1:1 RNA:protein (27,32,36–42). Our lab noted unusual effects in the reproducibility of SL3:NCp7 binding assays when [NaCl] $\leq$ 0.15M; we suggested that this was due to the presence of competing complexes with protein in excess (27). The current work was motivated by the need to distinguish conditions that cause the occurrence of $R_1P_1$ or $R_1P_{\geq 2}$ complexes, particularly as influenced by the nature and concentration of counterions, and to resolve disagreements in the literature regarding values for $K_d$ of the 1:1 complex. In addition, we provide a firm basis for characterizing the properties of $R_1P_1$ complexes that provide the specificity of packaging genomic RNA.

We show that metastable, non-equilibrium mixtures of protein-excess complexes can be rearranged to specific $R_1P_1$ complexes by increasing ionic strength, and that the persistence of metastable complexes can be influenced by the order of addition of RNA and protein at low ionic strength. Also, the metastable complexes can be eliminated by replacing $Na^+$ as the RNA counterion by $Mg^{2+}$; 0.018 M $Mg^{2+}$ added to the buffer used here produces the same $K_d$ as 0.200 M added $Na^+$. Other counterions are also explored. Lack of attention to these and other experimental details are shown to be a major source for disagreement among published $K_d$ values.

## EXPERIMENTAL PROCEDURES

### NCp7 preparation

The 55 amino acid NCp7 was prepared and the concentrations estimated as described in previous work (27,32). Protein stocks at 300 to 1,000 μM were stored for several months without degradation in a 25 mM acetate buffer, pH 5, with 10% glycerol, 10mM dithiothreitol, 0.05 mM EDTA, 25 mM NaCl, and 0.1 mM $ZnCl_2$ at −80°C. "AddNA" assays with SL3 added to 0.3 μM NCp7 were repeated as a positive control each day before performing any other

experiment (27,32). NCp7 preparations were rejected if they failed to exhibit at least 95% quenching with a three-fold excess of the 20mer, SL3-GGUG, GGACUAGC<u>GGUG</u>GCUAGUCC, which has $K_d = 10$ nM (32).

## SL3 RNA

SL3 was purchased from IDT DNA Technologies (Coralville, IA) and used without further purification. The RNA was heated to 95°C for 3 minutes, cooled on ice, and stored on ice prior to use.

## Fluorescence buffer

The buffer for the fluorescence assays contained 5.0 mM sodium phosphate ($Na_{1.38}H_{1.62}PO_4$; 5.0 mM $NaH_2PO_4$ was adjusted to pH 7.0 with NaOH), 0.10 mM $ZnCl_2$, 0.01% poly(ethylene glycol), and one of the added salts: NaCl, KCl, $NaC_2H_3O_2$, $MgCl_2$, $Na_2SO_4$, or $MgSO_4$, at concentrations specified in Figures 2–6. The ionic strength of each buffer is the contribution from the added salt plus 0.0091 M for sodium phosphate and $ZnCl_2$; ionic strength contributions are beyond the fourth decimal place for SL3-RNA and NCp7 at sub-micromolar concentrations. In this paper the buffer with 0.200 M added NaCl is referred to as the $\mu = 0.209$ M buffer, or by specifying only the nature and concentration of the added salt.

## AddNA assay

Ideal AddNA assays for 1:1 complexes are shown in supplementary Figure S1 to illustrate the expected response for a variety of $K_d$ values. Assays were performed by adding SL3 RNA (50 μM stock) in aliquots of 1.5–3 μL to 0.30 μM NCp7 in 2.00 mL of the fluorescence buffer in a 10×10 mm path length quartz fluorescence cuvette (NSG Precision Cells) along with an 8×1.5 mm stir bar. The fluorescence of the free NCp7 (i.e. the fraction of the protein not bound to SL3) was measured using a PTI QM-4/2003SE fluorometer at 349.9 nm emission using a 290 nm excitation, a 4 nm excitation band-pass and a 1.5–3 nm emission band-pass. The fluorescence titration curves obtained were fitted to a model assuming 1:1 stoichiometry for the ratio of NCp7 bound to SL3.

The titration curves were fitted to equation (1) as previously reported (32).

$$(I - I_\infty)/I_0 = \{-(\boldsymbol{R_t} - \boldsymbol{P_t} + K_d) + [(\boldsymbol{R_t} - \boldsymbol{P_t} + K_d)^2 + 4\boldsymbol{P_t}K_d]^{1/2}\}/2\boldsymbol{P_t} + I_\infty \tag{1}$$

$\boldsymbol{P_t}$ and $\boldsymbol{R_t}$ are total protein and total SL3 concentrations respectively, I is the measured fluorescence intensity, $I_0$ is the intensity when $\boldsymbol{R_t} = 0$, $I_\infty$ is the intensity at saturation, and $K_d$ is the dissociation constant. The equation was derived by using standard assumptions that I-$I_\infty$ is directly proportional to the free protein concentration, $\boldsymbol{P_f}$, that $\boldsymbol{P_t} = \boldsymbol{P_f} + \boldsymbol{P_{bound}}$, $\boldsymbol{R_t} = \boldsymbol{R_f} + \boldsymbol{R_{bound}}$, and $K_d = [\boldsymbol{R_f}][\boldsymbol{P_f}]/[\boldsymbol{R \cdot P}]$. The data were fitted using the OriginPro 7.5 software package; $\boldsymbol{P_t}$ was fixed at 0.30 μM, $I_\infty$ was fixed at zero, and $K_d$ was the only adjustable parameter. It was determined that there was no improvement in the fit by allowing $I_\infty$ to be an adjustable parameter. This is consistent with the >95% quenching standard for SL3-GGUG, described under *NCp7 preparation*, above.

## AddPro assay

Ideal AddPro assays for 1:1 complexes at constant $\boldsymbol{R_t} = 0.3$ μM are illustrated in Figure S2. Assays were performed by adding NCp7 (50 μM stock) in aliquots of 1.5–3 μL to 0.30 μM SL3 in 2.00 mL of the fluorescence buffer (0.010 to 0.800 M added NaCl), and fluorescence

measured as for the AddNA assays, above. At NaCl concentrations lower than 0.15 M the starting concentrations of SL3 and NCp7 were diluted 4-fold to move the titration curves away from the 1:1 line.

Fitting details are similar to the AddNA titrations, except the data were fitted to equation (2).

$$I - I_0 = m\{P_t - R_d - K_d + [(R_t + P_t + K_d)^2 + 4R_t P_t]^{1/2}\}/2 \tag{2}$$

The parameters are the same as in equation (1), except that m is the slope of plots when no interaction occurs or when no RNA is present, and $I_0$ is the blank intensity. The data were fitted using OriginPro 7.5 with $R_t$ fixed at the starting value (0.30 or 0.075 μM), and $K_d$ and m as the adjustable parameters. Fitting was less reproducible if m was not an adjustable parameter.

### Alternative counterions

AddNA assays were performed to assess the effect of $K^+$, $Mg^{2+}$, $OAc^-$ (acetate), and $SO_4^{2-}$ ions on the binding equilibria. Reagent grade crystals of NaCl, KCl, $MgCl_2$, $Na_2SO_4$, and $MgSO_4$ were used. Standardized solutions of NaOH were mixed with standardized acetic acid to achieve accurate concentrations of NaOAc as the salt is strongly deliquescent (1.000 M solutions of NaOH and HOAc were purchased from Sigma-Aldrich, and 2.000 M solutions from Ricca Chemical Co.).

## RESULTS

### Validation of AddPro assays

Prior to the use of AddPro assays, their usefulness should be validated with respect to traditional AddNA titrations. Figures 2 and 3 compare AddNA and AddPro under conditions where the AddNA data signify the formation of a 1:1 complex between SL3-RNA and NCp7 (27, 32). In both Figures the points that lie nearest the long-dashed 1:1 line are for complexes that have the highest affinity (lowest salt), with isotherms rising progressively higher as salt concentration increases (the long-dashed line denotes a complex where the binding constant ($1/K_d$) approaches infinity). In the AddNA assays the total RNA concentration, $R_t$, increases from left to right along the horizontal axis; $R_t/P_t$ is the mole ratio of total RNA over total protein, and $P_t = 0.30$ μM is held constant. AddPro assays have $P_t$, increasing from left to right, holding $R_t$ constant at 0.30 μM and again varying [NaCl]. As salt concentration increases above 0.2 M, the affinity decreases as expected for the association of the highly charged protein and RNA. The legends to Figs. 2 and 3 give the best-fit $K_d$ values for these particular datasets; the agreement between the two assays is excellent at [NaCl] = 0.2 and 0.3 M, but the $K_d$ values agree less well at higher salt. As can be seen from Fig. 3, AddPro assays exhibit very little difference between the data points at [NaCl] ≥ 0.5 M and the "no binding" limit line (short dashes). Near this limit the fitting is very sensitive to small deviations in the experimental data. Thus, AddPro $K_d$ values at high salt are less reproducible than for [NaCl] values near 0.2 M. It is also true that the fits for AddNA titrations at high salt are less reliable than those near 0.2 M salt as the fluorescence intensities at right end of the binding isotherms measured at high salt do not approach the limit, $I_\infty$, characteristic of an RNA-saturated 1:1 complex. The general result is that the AddPro assays give the same $K_d$ values as AddNA assays within experimental error. Importantly, the order of addition of RNA and protein is irrelevant in the physiological range of salt concentration, consistent with 1:1 complex in rapid equilibrium with free RNA and protein.

## Order of addition of RNA and protein at low salt

The issues that occur at lower ionic strength in AddNA assays are illustrated in Figure 4. The data measured at 0.100 and 0.150 M [NaCl] (Fig. 4a) fall between the lines for complexes with stoichiometry of 1:1 (long dashes) and 1:2 (short dashes). This indicates that a persistent complex with an excess of protein over RNA ($R_1P_{n>1}$) occurs in addition to $R_1P_1$ when RNA is added to protein at low salt. (As a reference, the upper data set (diamonds) shows the average of three replicate trials in 0.200 M added NaCl in the fluorescence buffer. These points all lie above the heavy-dashed line, as expected for 1:1 complexes, and the error bars are small.) Data at 0.050 M NaCl (Fig. S3) also fall between the 1:1 and 1:2 lines, but are not even reproducible from one day to the next. Adding 2.00 M NaCl solution to make the final [NaCl] = 0.200 M moves any of the data points below the 1:1 line to the 0.200 M titration curve at the corresponding $R_t/P_t$ ratio (see Figure 4b); this change occurs within the few seconds required for addition and mixing.

By contrast, the AddPro assays for 0.150 M NaCl (open triangles in Fig. 3), and for 0.100 and 0.050 M NaCl (Fig. 5) all fall near the 1:1 line, but above it, consistent with 1:1 complexes having high affinity. Thus, when protein is added to RNA, $R_1P_{n>1}$ complexes do not form in this range of salt concentrations, and equilibration is rapid. At very low salt concentrations (0.010 and 0.025 M NaCl) AddPro titrations also produce mixed $R_1P_1$ and $R_1P_{n>1}$ complexes (Figure S4). Thus, the region of salt where persistent $R_1P_{n>1}$ complexes can occur is [NaCl] < 0.200 M, at least in the sub-micromolar range of $R_t$ and $P_t$ employed in this work. That persistent $R_1P_{n>1}$ complexes occur only in the AddNA titrations when [NaCl] is between 0.050–0.15 M is diagnostic of a non-equilibrium situation when RNA is added to protein. This, and the persistence of non-equilibrium mixtures of $R_1P_{n>1}$, and $R_1P_1$ complexes at even lower salt concentrations, calls into doubt many previous determinations of affinity assumed to be for $R_1P_1$ complexes (see Discussion).

Averages of replicate determinations of $K_d$ for the 1:1 complex are reported in the first three columns of Table 1 at several concentrations of NaCl. $K_d$ values at [NaCl] < 0.200 M are from AddPro assays, whereas values at [NaCl] > 0.300 M are from AddNA data. $K_d$ values averaged in Table 1 for 0.100 and 0.050M NaCl are from AddPro measurements at $R_t$ = 0.075 μM.

## Global variation in ionic strength

The entire set of data used for determinations of $K_d$ in NaCl, KCl, NaOAc, $MgCl_2$, $Na_2SO_4$, and $MgSO_4$ are encompassed in Figure 6. Individual titrations for the latter five salts are not shown, but $K_d$ values were calculated exclusively from AddNA assays. Highest affinities of NCp7 for SL3 are at the top of the y-axis, and the highest salt concentrations are at the right of the x-axis. Contributions to the ionic strength for the salts used in this work are,

$$\mu_{salt} = 0.5([C]Z_C^2 + [A]Z_A^2) \tag{3}$$

where C is the cation and A is the anion of the salt in question, and $Z_C$ and $Z_A$ are the charges on the respective ions. For the singly charged ions in NaCl, KCl, and NaOAc, $\mu_{salt}$ equals the molar concentration. The total ionic strength, μ, is the sum of $\mu_{salt}$ plus 0.009 M, which is the contribution to the ionic strength from the buffer components. Slopes of the best fit lines for each salt are given in the legend to Fig. 6.

The AddPro assays in NaCl give access to binding constants, $(K_d)^{-1}$, that are nearly two orders of magnitude higher than can be surveyed using AddNA assays (data points at the top of Fig. 6). The whole collection of data points in NaCl include those measured in this work by AddPro (open triangles) and AddNA (open diamonds), and previously (27) by AddNA (open circles).

The slopes of the best-fit lines provide a different sort of average from replicate measurements, now over all of the data for a given salt. There is good agreement between these two averages, reflecting the high quality of the measurements. The slopes can be used to predict $K_d$ at any salt concentration. The predictions for NaCl are compared with the replicate averaged $K_d$ values in the last column of Table 1. These averages compare reasonably well, especially at intermediate salt concentrations. A prediction of $K_d$ = 22 pM for [NaCl] = 0.010 M is also included in the table. However, attempts to measure this value failed as the titrations were irreproducible from day to day in a manner reminiscent of the AddNA assays at low salt (see Figs. S3 and S4).

## Nature of the salt

Plots of $K_d$ as a function of ionic strength for the other salts are also shown in Fig. 6. The data for KCl ($\times$) are found among the data points for NaCl, showing that no large change in the affinity of the complex occurred upon substituting $K^+$ for $Na^+$. However, substituting acetate ion (open squares) for chloride resulted in a substantial displacement from the NaCl line. As the two best-fit lines have nearly the same slope, it can be seen that the complex in $OAc^-$ has about half the $K_d$ as it has in $Cl^-$, *i.e.*, acetate makes the complex about twice as stable at the same ionic strength (2.3 times more stable at $\mu$ = 0.209 M).

Substituting doubly charged ions for either $Na^+$ or $Cl^-$ produces a substantial displacement of the best-fit lines in Fig. 6. Sulfate stabilizes the complex (filled circles) even more than $OAc^-$, whereas replacing sodium with magnesium at the same ionic strength strongly destabilizes the complex (filled triangles). $MgSO_4$ shows intermediate behavior (filled diamonds), with the destabilizing effect of $Mg^{2+}$ dominating the stabilizing effect of $SO_4^{2-}$. All of these data sets exhibit curvature about the best-fit straight lines. This is expected as deviations from ideal solutions are more severe for multiply charged ions, especially at higher ionic strengths. The dashed line in Fig. 6 was fitted to the $MgCl_2$ data for ionic strengths at and below 0.129 M (40 mM added $MgCl_2$). A thin horizontal line connects the dashed line to the best-fit line for NaCl at 0.200 M added NaCl. This equivalence in $K_d$ occurs at 18 ±3 mM added $MgCl_2$ ($\mu$ = 0.063 M including the buffer salts).

# DISCUSSION

The stoichiometry and affinity of NCp7-SL3 complexes depend on the relative contributions of specific binding to the loop bases in SL3 RNA and ionic interactions that are not sequence-specific. The ionic contribution is most profoundly affected by the concentration and nature of added salts. Below 0.200 M NaCl, the order of addition of RNA and protein can lead to the formation of persistent, non-equilibrium (metastable) mixtures of $R_1P_{n>1}$ and $R_1P_1$ complexes. Variation in the RNA or protein sequence, especially mutations that decrease the stability of the 1:1 complex, play a role in the distribution of complexes, as well (43). A better understanding of these effects, discussed in the next several paragraphs, explains much of the disagreement in reported $K_d$ values for SL3-NCp7 interaction, (22,27,31–32,[36]–[38],41–42,44–45).

## Effect of NaCl concentration

It is well-known that high salt concentrations suppress ionic interactions. Due to the high charges on fully ionized SL3 (−19) and NCp7 (+9; see legend to Fig. 1), ionic effects will contribute substantially to the stability of both specific $R_1P_1$ and non-specific $R_1P_{n>1}$ complexes. The latter should be most dependent on salt concentration as more ionic interactions are neutralized in the complex. The charge on SL3 RNA is reduced by counterion condensation and the charges on both RNA and protein are screened by their respective counterion atmospheres. Condensation of sodium ions on SL3 in NaCl should reduce the net charge to −5

to −6 ((46); the range arises from assumptions regarding the loop phosphates). Of course, many counterions are released when a complex forms. For instance, six salt-bridge interactions were seen between SL3-phosphates and basic side-chains of NCp7 in the NMR structure (31). Other phosphates are buried in the electropositive binding surface of the protein, as well. Thus, the $R_1P_1$ complex is likely to retain a substantial net negative charge. A fully ionized $R_1P_2$ complex would have a charge of −1, which is very near electrical neutrality. Such a complex is likely to have low solubility and is a likely contributor to metastable mixtures. These concepts are borne out by the experiments summarized in Results.

Data presented in Figs. 2, 3 show that when $[NaCl] \geq 0.2M$ the specific $R_1P_1$ complex is formed. However, nonspecific binding ($R_1P_{n>1}$ complexes) becomes significant in AddNA assays monitored by fluorescence at $[NaCl] \leq 0.15$ M (see Figs. 4 and S3) and AddPro assays at $[NaCl] < 0.05$ M (see Fig. S4). Early points in AddNA titrations have very little RNA and a large excess of protein. This would favor the production of sparingly soluble $R_1P_{n>1}$ complexes that may rearrange slowly upon further addition of RNA. Of course, low salt also favors unfolding of the RNA hairpin, and primarily electrostatic interaction with two or more proteins at non-sequence-specific binding sites. The appearance of $R_1P_{n>1}$ complexes at $[NaCl] < 0.05$ M in AddPro titrations could be due to the high concentration of protein in the microliter droplets that are added to the RNA solution – $R_1P_{n>1}$ complexes could form near the surface of droplets, and rearrange only slowly, thereafter.

As expected, the electrostatic attraction between RNA and protein produces a large increase in the affinity of the specific 1:1 complex upon decreasing the salt concentration. The binding constant, $1/K_d$, changes by $\sim 10^4$ per factor of ten difference in salt concentration for NaCl, KCl, and NaOAc (see Table 1, Fig. 6).

A consequence of using SL3 in AddNA assays as a daily positive control is that a large number of replicates was available to reduce the standard deviation on the average $K_d = 21 \pm 2$ nM (N = 38). The new average value is somewhat lower than was reported earlier, $28 \pm 6$ nM (32), which was obtained from fewer determinations and using the solver function in Microsoft Excel. The nonlinear optimization routine in the Origin software is superior to that in Excel. Thus, we report $K_d = 21 \pm 2$ nM, as definitive in 0.200 M NaCl plus the $\mu = 0.009$ M buffer for the sequences shown in Fig. 1.

## Alternative counterions

$Mg^{2+}$ ions are known to stabilize double helices more than $Na^+$, which should disfavor two or more proteins binding to open the helical stem to form non-specific complexes. Also, divalent ions in the counterion atmosphere screen electrostatic interactions more effectively than monovalent ions. Our results showed that divalent $Mg^{2+}$ ions shift the distribution of species away from $R_1P_{n>1}$ complexes to form exclusively $R_1P_1$ complexes over the full range of ionic strengths examined for $MgCl_2$ (0.05 to 0.3 M). We also noted with regard to Fig. 6 that adding 18 mM $MgCl_2$ to the $\mu = 0.009$ M buffer produced the same 1:1 binding affinity as adding 200 mM NaCl. There are situations, *e.g.*, in NMR spectroscopy, where there is an advantage to use 18 mM $MgCl_2$ in the buffer, and maintain equivalence to the affinity observed for nearly physiological salt concentrations, while disfavoring the formation of $R_1P_{n>1}$ complexes (43).

Both acetate and sulfate ions increase the stability of $R_1P_1$ complexes over chloride, although the destabilization by $Mg^{2+}$ is much larger in solutions at the same ionic strength. Perhaps $OAc^-$ and $SO_4^{2-}$ are better able to stabilize the protein in its binding conformation compared to $Cl^-$. Although NC-bound $SO_4^{2-}$ should efficiently screen the ionic attraction between SL3 and NCp7, this destabilizing effect is apparently outweighed by the stabilizing influence that sulfate confers on the protein in the complex.

## Stoichiometry

The stoichiometry of the complexes is an important issue. Figures 4. S1–S4 show that $R_1P_{n>1}$ complexes or their mixtures with $R_1P_1$ can be easily distinguished from 1:1 complexes in the W37 fluorescence-based assays. $R_1P_1$, $R_1P_2$, and $R_1P_3$ complexes have been observed by mass spectrometry (MS) for SL3 in the presence of excess NCp7 (41). For the DNA octamer, $[d(TG)]_4$, observations by surface plasmon resonance (SPR) and MS have shown that both $D_1P_1$, and $D_1P_2$ complexes form in interactions with NCp7 complexes; the affinity for the second protein is ∼5 times less than in the formation of $D_1P_1$ as determined by SPR (42).

Diagnosing the presence of complexes with $R_{n>1}P_1$ stoichiometries is problematic using the W37-fluorescence assays, where binding only the first high affinity RNA can completely quench the fluorescence. $D_2P_1$ complexes have been observed by SPR, where the affinity of NCp7 for the second $[d(TG)]_4$ is ∼300 times less than for the first; this much lower affinity $D_2P_1$ complex was not observed by mass spectrometry (MS) in the same report (42). Likewise, $R_{n>1}P_1$ complexes were not observed by MS for SL3-NCp7 (41). Therefore, it is likely that excess-RNA complexes can be ignored in studies of the sequence-specific interactions of SL3 with NCp7 in 0.2 M NaCl or 18 mM $MgCl_2$, and in the specific packaging of HIV-1 RNA by NC-domains of gag and gag-pol precursors.

## Effects of non-ideality

Several cautions are worth noting with regard to effects on the complexes due to the nature and concentrations of salt, protein, and nucleic acid. (i) Deviations from ideal solution characteristics are large for charged molecules. For instance, at ionic strengths of 0.3 M the mean ionic activity coefficient, $\gamma_\pm$, is near 0.7 for NaCl (47), KCl (48), and NaOAc (49); near 0.5 for $MgCl_2$ (50) and $Na_2SO_4$ (51); and near 0.2 for $MgSO_4$ (49). The practical significance is that each increment of added salt produces a smaller effect on $K_d$ at higher salt concentrations than at lower concentrations. In plots such as in Fig. 6, this leads to curvature, with a higher slope at low salt concentrations. That is why we used data only at $\mu \leq 0.129$ M for $MgCl_2$ (dashed line in Fig. 6), to find the $[MgCl_2]$ that produces $K_d$ equivalent to that in 0.200 M added NaCl. (ii) Effects due to non-ideal solutions are most severe for highly charged species, so it should be expected that concentration-based equilibrium constants (as opposed to activity-based equilibria, which regulate the bound and free protein and nucleic acid species), will vary with concentration of the macromolecules. Non-ideality should exert a greater effect at higher concentrations of protein and nucleic acid. (iii) Experimental techniques for measuring $K_d$ values are often limited to windows in concentration that do not overlap with each other. NMR concentrations are typically 300–3,000× that used in this work, isothermal titration calorimetry (ITC, 500×, (45)), and mass spectrometry (MS, 30–60×, (41)). Effects due to non-ideality could make it difficult to compare the results of experiments measured in these widely differing concentration ranges.

## Sample integrity

Perhaps the greatest single caution regarding future work is the importance of positive controls on the integrity of preparations of SL3, and especially, NCp7 (see Experimental). The experience in our laboratory is that a stock solution of NCp7 may be frozen and thawed many times, but eventually undergoes a rapid collapse in its affinity for SL3. Thus, fluorescence-AddNA assays with SL3 in the $\mu = 0.209$ M buffer + NaCl should be repeated each day before performing any other experiment. NCp7 degradation may be the most common source of $K_d$ values reported in the literature that are substantially higher than the predictions in Fig. 6 for $\mu \geq 0.2$ M.

## Comparison with published analyses of the SL3-NCp7 interaction

Including their own report, Hagan & Fabris (41) collected data from ten publications on the $K_d$ and stoichiometry of SL3-NC complexes. More recently, $R_1P_{n>1}$ complexes were observed at low [NaCl] using electron paramagnetic resonance (EPR), which changed to $R_1P_1$ at higher salt (44) in concordance with our results reported here. In these eleven studies the SL3-NC equilibrium was probed by seven methods in four different salt concentrations (see Table 1 in ref. (41)). The results differ widely. The leading cause of the variation is that eight studies were conducted at $\mu \leq 0.05$ M, where the present work has demonstrated the common occurrence of $R_1P_{n>1}$ complexes and metastable mixtures of $R_1P_{n>1}$ and $R_1P_1$ complexes. Other causes may include effects due to non-ideality or that some measurements may have been compromised by insufficient positive controls on the integrity of NCp7 and SL3. Also, several of the studies were conducted in unbuffered solutions or at pH values outside the buffering range of the salts added to the solutions, *e.g.*, NaOAc at pH 6 to 8 (the effect of pH on SL3-NC stoichiometry and affinity has not been determined). We have discussed most of this work previously (27,32), and now consider two studies further (41,45).

In the first study, intensities of ions derived from SL3, NCp7, and their $R_1P_1$, $R_1P_2$, and $R_1P_3$ complexes were measured using electrospray ionization mass spectrometry (41). They reported $K_d = 180 \pm 60$ nM for the 1:1 complex in 0.15 M NaOAc (pH 7.5; no buffer or details of adjusting pH were specified). The dependence of $K_d$ on [NaOAc] in Fig. 6 of the current work can be used to predict that $K_d = 3$ nM in a buffer that is equivalent to the salt conditions in reference (41). The authors suggested that quantification by MS is superior to methods that require curve fitting to determine $K_d$, such as W37-fluorescence assays. On the other hand, there is great confidence in the W37-assays because, (i) assays with SL3 and SL3-GGUG in the $\mu = 0.209$ M buffer exhibit nearly 100% quenching of W37, consistent with an almost perfectly linear correlation between the fluorescence intensity and the free protein concentration, and (ii) the known 3D structure provides a clear mechanism for full quenching by stacking W37 on G318 of SL3. The 60-fold difference in $K_d$ cannot be due to curve fitting errors. In fact, the $K_d$ value measured by ESI MS came from curve fitting to a competition experiment with a variant of SL4, which was separately determined to have $K_d = 1,300 \pm 500$ nM (41). Examination of Fig. 3 in (41) shows that the data show only approximate agreement between the measured intensities and the fitted binding isotherm for the SL4 complex. Resorting to a competition assay is necessitated by the relative insensitivity of the method to directly assay high affinity complexes and their unbound components. Furthermore, it is an open question whether ionization efficiencies are sufficiently constant to accurately sample the equilibrium populations. Nevertheless, the MS work is clearly valuable due to its unequivocal demonstration of the presence of $R_1P_{n\geq1}$ complexes when $\boldsymbol{P_t} > \boldsymbol{R_t}$ and the insignificance of $R_{n\geq1}P_1$ complexes in the SL3-NCp7 system.

In the second study, there is a 2,500-fold difference in the value of $K_d = 170$ nM measured by ITC (45) at $\mu = 0.05$ M, and $K_d = 0.07$ nM extrapolated from Fig. 6. Although the $K_d$ values of the MS (180 nM) and ITC experiments (170 nM) appear numerically close to each other, the agreement is fortuitous as the solutions differed in ionic strength by a factor of three. Using the slope of the NaOAc line in Fig. 6 shows that these $K_d$ values actually differ from each other by 60-fold when corrected for ionic strength due to the small ions. Work in progress in our laboratory is aimed at reconciling differences between $K_d$ measurements made by ITC, SPR, electrophoretic mobility shifts, and W37-fluorescence.

## Implications for drug discovery

Beyond an interest to accurately define $K_d$ and conditions for study of the 1:1 complex, the simple expedient of comparing affinities at 0.2 M NaCl or 18 mM $MgCl_2$ is sufficient to

suppress the non-sequence-specific interactions to the point that anti-NC agents can be found to interrupt the specific interactions (43,52–53).

## Implications for packaging specificity

In vitro measurements of NC interactions with RNA and DNA show that the interactions with unpaired bases are much stronger than with paired strands (35–36,42,54). Measuring the affinity for SS RNA is complicated because multiple NCp7 moieties can bind sequences that are longer than 5–6 unpaired nt (35–36,42,55). In previous work we have measured the $K_d$ values of NCp7 for 35 of the 64 GNNN variants of the wild-type GGAG loop on the SL3 RNA stem at 0.2 M NaCl (32,55). The data can be used to predict that the overall average affinity for these single-stranded loops is $K_d = 2,500$ nM. Thus, specific affinity for the GGAG loop is about 100 times greater than the average of these four-base loops. This ratio of specific vs. non-specific binding is comparable to many other biological interactions, and probably more than sufficient for HIV-1 to package its full-length RNA over non-genomic fragments and non-viral mRNA. This ratio of specific to non-specific affinity is similar to the antibiotic, paromomycin, which has ~100-fold higher affinity for the decoding region A-site of ribosomal RNA compared to non-specific binding to competing secondary sites (56).

## Implications for chaperone activity

Rapid rearrangement of protein-nucleic acid complexes is one of the major components of the NC nucleic acid chaperone function (5,11,57). In Results we reported that adding concentrated NaCl to $R_1P_{n>1}$ at low salt produced a rapid rearrangement to $R_1P_1$ even in the presence of excess protein. It is apparent that the collection of free and bound species can rearrange within seconds to changes in the balance of specific and electrostatic interactions. This is supported by NMR observations (45), which showed that free and bound SL3 and NCp7 exhibit exchange-crosspeaks having a dissociation rate constant of 5 $s^{-1}$.

## Implications for analysis of condensed RNA-NCp7 interactions

Recent analyses of spin-labeled SL3 interacting with NCp7 at low salt have been shown by EPR to have intriguing properties that should be similar to genomic RNA in mature virions (44). AddPro titrations similar to those described in Fig. S4 may be useful in guiding the construction of nearly pure $R_1P_2$ complexes.

# Supplementary Material

Refer to Web version on PubMed Central for supplementary material.

# Acknowledgments

# ABBREVIATIONS AND TEXTUAL FOOTNOTE

| | |
|---|---|
| SL3 | stem-loop 3 with unpaired residues at G317-G318-A319-G-320 of the 5′-leader of HIV-1 genomic RNA |
| NCp7 | HIV-1 nucleocapsid protein |
| $K_d$ | equilibrium constant for the dissociation of a bimolecular complex |
| $P_t$ | total concentration of protein |
| $R_t$ | total strand concentration of RNA |

MS          mass spectrometry

ESI         electrospray ionization

SPR         surface plasmon resonance

ITC         isothermal titration calorimetry

## References

1. Linial ML, Miller AD. Retroviral RNA packaging: sequence requirements and implications. Curr Top Microbiol Immunol 1990;157:125–152. [PubMed: 2394131]

2. Wills JW, Craven RC. Form, function, and use of retroviral gag proteins. Aids 1991;5:639–654. [PubMed: 1883539]

3. Oertle S, Spahr PF. Role of the gag polyprotein precursor in packaging and maturation of Rous sarcoma virus genomic RNA. J Virol 1990;64:5757–5763. [PubMed: 1700822]

4. Damgaard CK, Dyhr-Mikkelsen H, Kjems J. Mapping the RNA binding sites for human immunodeficiency virus type-1 gag and NC proteins within the complete HIV-1 and -2 untranslated leader regions. Nucleic Acids Res 1998;26:3667–3676. [PubMed: 9685481]

5. Williams MC, Rouzina I, Wenner JR, Gorelick RJ, Musier-Forsyth K, Bloomfield VA. Mechanism for nucleic acid chaperone activity of HIV-1 nucleocapsid protein revealed by single molecule stretching. Proc Natl Acad Sci U S A 2001;8:8.

6. Darlix JL, Cristofari G, Rau M, Pechoux C, Berthoux L, Roques B. Nucleocapsid protein of human immunodeficiency virus as a model protein with chaperoning functions and as a target for antiviral drugs. Adv Pharmacol 2000;48:345–372. [PubMed: 10987096]

7. Muriaux D, De Rocquigny H, Roques BP, Paoletti J. NCp7 activates HIV-1Lai RNA dimerization by converting a transient loop- loop complex into a stable dimer. J Biol Chem 1996;271:33686–33692. [PubMed: 8969239]

8. Fu W, Gorelick RJ, Rein A. Characterization of human immunodeficiency virus type 1 dimeric RNA from wild-type and protease-defective virions. J Virol 1994;68:5013–5018. [PubMed: 8035501]

9. Rist MJ, Marino JP. Mechanism of Nucleocapsid Protein Catalyzed Structural Isomerization of the Dimerization Initiation Site of HIV-1. Biochemistry 2002;41:14762–14770. [PubMed: 12475224]

10. Prats AC, Sarih L, Gabus C, Litvak S, Keith G, Darlix JL. Small finger protein of avian and murine retroviruses has nucleic acid annealing activity and positions the replication primer tRNA onto genomic RNA. Embo J 1988;7:1777–1783. [PubMed: 2458920]

11. Hargittai MR, Gorelick RJ, Rouzina I, Musier-Forsyth K. Mechanistic insights into the kinetics of HIV-1 nucleocapsid protein-facilitated tRNA annealing to the primer binding site. J Mol Biol 2004;337:951–968. [PubMed: 15033363]

12. Druillennec S, Caneparo A, de Rocquigny H, Roques BP. Evidence of interactions between the nucleocapsid protein NCp7 and the reverse transcriptase of HIV-1. J Biol Chem 1999;274:11283–11288. [PubMed: 10196217]

13. Lener D, Tanchou V, Roques BP, Le Grice SF, Darlix JL. Involvement of HIV-I nucleocapsid protein in the recruitment of reverse transcriptase into nucleoprotein complexes formed in vitro. J Biol Chem 1998;273:33781–33786. [PubMed: 9837967]

14. de Rocquigny H, Caneparo A, Delaunay T, Bischerour J, Mouscadet JF, Roques BP. Interactions of the C-terminus of viral protein R with nucleic acids are modulated by its N-terminus. Eur J Biochem 2000;267:3654–3660. [PubMed: 10848983]

15. Berthoux L, Pechoux C, Darlix JL. Multiple effects of an anti-human immunodeficiency virus nucleocapsid inhibitor on virus morphology and replication. J Virol 1999;73:10000–10009. [PubMed: 10559314]

16. Stephen AG, Rein A, Fisher RJ, Shoemaker RH. The nucleocapsid protein as a target for novel anti-HIV drugs. Current Drug Discovery 2003 August;:33–36.

17. Yuan Y, Kerwood DJ, Paoletti AC, Shubsda MF, Borer PN. Stem of SL1 RNA in HIV-1: Structure and Nucleocapsid Protein Binding for a $1 \times 3$ Internal Loop. Biochemistry 2003;42:5259–5269. [PubMed: 12731867]

18. Cruceanu M, Stephen AG, Beuning PJ, Gorelick RJ, Fisher RJ, Williams MC. Single DNA molecule stretching measures the activity of chemicals that target the HIV-1 nucleocapsid protein. Analytical biochemistry 2006;358:159–170. [PubMed: 17034752]

19. Vogt VM, Simon MN. Mass determination of rous sarcoma virus virions by scanning transmission electron microscopy. J Virol 1999;73:7050–7055. [PubMed: 10400808]

20. Coffin, JM.; Hughes, SH.; Varmus, HE. Retroviruses. Cold Spring Harbor Lab Press; Plainview, NY: 1997.

21. Gelderblom HR. Assembly and morphology of HIV: potential effect of structure on viral function. Aids 1991;5:617–637. [PubMed: 1652977]

22. Clever J, Sassetti C, Parslow TG. RNA secondary structure and binding sites for gag gene products in the 5′ packaging signal of human immunodeficiency virus type 1. J Virol 1995;69:2101–2109. [PubMed: 7884856]

23. Clever JL, Eckstein DA, Parslow TG. Genetic dissociation of the encapsidation and reverse transcription functions in the 5′ R region of human immunodeficiency virus type 1. J Virol 1999;73:101–109. [PubMed: 9847312]

24. Clever JL, Parslow TG. Mutant human immunodeficiency virus type 1 genomes with defects in RNA dimerization or encapsidation. J Virol 1997;71:3407–3414. [PubMed: 9094610]

25. McBride MS, Panganiban AT. The human immunodeficiency virus type 1 encapsidation site is a multipartite RNA element composed of functional hairpin structures. J Virol 1996;70:2963–2973. [PubMed: 8627772]

26. McBride MS, Schwartz MD, Panganiban AT. Efficient encapsidation of human immunodeficiency virus type 1 vectors and further characterization of cis elements required for encapsidation. J Virol 1997;71:4544–4554. [PubMed: 9151848]

27. Shubsda MF, Paoletti AC, Hudson BS, Borer PN. Affinities of Packaging Domain Loops in HIV-1 RNA for the Nucleocapsid Protein. Biochemistry 2002;41:5276–5282. [PubMed: 11955077]

28. Darlix JL, Lapadat-Tapolsky M, de Rocquigny H, Roques BP. First glimpses at structure-function relationships of the nucleocapsid protein of retroviruses. J Mol Biol 1995;254:523–537. [PubMed: 7500330]

29. Hayashi T, Ueno Y, Okamoto T. Elucidation of a conserved RNA stem-loop structure in the packaging signal of human immunodeficiency virus type 1. FEBS Lett 1993;327:213–218. [PubMed: 8335111]

30. Hayashi T, Shioda T, Iwakura Y, Shibuta H. RNA packaging signal of human immunodeficiency virus type 1. Virology 1992;188:590–599. [PubMed: 1585635]

31. De Guzman RN, Wu ZR, Stalling CC, Pappalardo L, Borer PN, Summers MF. Structure of the HIV-1 nucleocapsid protein bound to the SL3 psi-RNA recognition element. Science 1998;279:384–388. [PubMed: 9430589]

32. Paoletti AC, Shubsda MF, Hudson BS, Borer PN. Affinities of the Nucleocapsid Protein for Variants of SL3 RNA in HIV-1. Biochemistry 2002;41:15423–15428. [PubMed: 12484783]

33. Summers MF, Henderson LE, Chance MR, Bess JW, South TL, Blake PR, Sagi I, Perez-Alvarado G, Sowder RC, Hare I DR, Arthur LO. Nucleocapsid zinc fingers detected in retroviruses: EXAFS studies of intact viruses and the solution-state structure of the nucleocapsid protein from HIV-1. Protein Sci 1992;1:563–574. [PubMed: 1304355]

34. Cornille F, Mely Y, Ficheux D, Savignol I, Gerard D, Darlix JL, Fournie-Zaluski MC, Roques BP. Solid phase synthesis of the retroviral nucleocapsid protein NCp10 of Moloney murine leukaemia virus and related "zinc-fingers" in free SH forms. Influence of zinc chelation on structural and biochemical properties. Int J Pept Protein Res 1990;36:551–558. [PubMed: 1708745]

35. Vuilleumier C, Bombarda E, Morellet N, Gerard D, Roques BP, Mely Y. Nucleic acid sequence discrimination by the HIV-1 nucleocapsid protein NCp7: a fluorescence study. Biochemistry 1999;38:16816–16825. [PubMed: 10606514]

36. Fisher RJ, Rein A, Fivash M, Urbaneja MA, Casas-Finet JR, Medaglia M, Henderson LE. Sequence-specific binding of human immunodeficiency virus type 1 nucleocapsid protein to short oligonucleotides. J Virol 1998;72:1902–1909. [PubMed: 9499042]

37. Shubsda MF, Kirk CA, Goodisman J, Dabrowiak JC. Binding of human immunodeficiency virus type 1 nucleocapsid protein to psi-RNA-SL3. Biophysical chemistry 2000;87:149–165. [PubMed: 11099178]

38. Maki AH, Ozarowski A, Misra A, Urbaneja MA, Casas-Finet JR. Phosphorescence and Optically Detected Magnetic Resonance of HIV-1 Nucleocapsid Protein Complexes with Stem-Loop Sequences of the Genomic Psi-Recognition Element. Biochemistry 2001;40:1403–1412. [PubMed: 11170468]

39. Amarasinghe GK, Zhou J, Miskimon M, Chancellor KJ, McDonald JA, Matthews AG, Miller RR, Rouse MD, Summers MF. Stem-loop SL4 of the HIV-1 psi RNA packaging signal exhibits weak affinity for the nucleocapsid protein. structural studies and implications for genome recognition. J Mol Biol 2001;314:961–970. [PubMed: 11743714]

40. Urbaneja MA, Wu M, Casas-Finet JR, Karpel RL. HIV-1 nucleocapsid protein as a nucleic acid chaperone: spectroscopic study of its helix-destabilizing properties, structural binding specificity, and annealing activity. J Mol Biol 2002;318:749–764. [PubMed: 12054820]

41. Hagan N, Fabris D. Direct mass spectrometric determination of the stoichiometry and binding affinity of the complexes between nucleocapsid protein and RNA stem-loop hairpins of the HIV-1 Psi-recognition element. Biochemistry 2003;42:10736–10745. [PubMed: 12962498]

42. Fisher RJ, Fivash MJ, Stephen AG, Hagan NA, Shenoy SR, Medaglia MV, Smith LR, Worthy KM, Simpson JT, Shoemaker R, McNitt KL, Johnson DG, Hixson CV, Gorelick RJ, Fabris D, Henderson LE, Rein A. Complex interactions of HIV-1 nucleocapsid protein with oligonucleotides. Nucleic Acids Res 2006;34:472–484. [PubMed: 16434700]

43. Yang, L. PhD dissertation. Syracuse University; 2008. NMR analysis of structural features of the HIV-1 nucleocapsid protein in response to mutation and interaction with RNA and drug candidates.

44. Xi X, Sun Y, Karim CB, Grigoryants VM, Scholes CP. HIV-1 nucleocapsid protein NCp7 and its RNA stem loop 3 partner: rotational dynamics of spin-labeled RNA stem loop 3. Biochemistry 2008;47:10099–10110. [PubMed: 18729386]

45. Amarasinghe GK, De Guzman RN, Turner RB, Chancellor KJ, Wu ZR, Summers MF. NMR structure of the HIV-1 nucleocapsid protein bound to stem-loop SL2 of the psi-RNA packaging signal. Implications for genome recognition. J Mol Biol 2000;301:491–511. [PubMed: 10926523]

46. Cantor, CR.; Schimmel, PR. The behavior of biological macromolecules. Vol. Part III. W.H. Freeman; San Francisco: 1980. Biophysical Chemistry.

47. Truesdell AH. Activity Coefficients of Aqueous Sodium Chloride from 15{degrees} to 50{degrees} C Measured with a Glass Electrode. Science 1968;161:884–886. [PubMed: 17812114]

48. Hostetler PB, Truesdell AH, Christ CL. Activity Coefficients of Aqueous Potassium Chloride Measured with a Potassium-Sensitive Glass Electrode. Science 1967;155:1537–1539. [PubMed: 17830046]

49. Weast, RC.; Astle, MJ. CRC Handbook of Chemistry and Physics. 63. CRC Press; Boca Raton, Fl: 1982.

50. Stokes RH, Robinson RA. Ionic hydration and activity in electrolyte solutions. J Am Chem Soc 1948;70:1870–1878. [PubMed: 18861802]

51. Robinson, RA.; Stokes, RH. Electrolyte Solutions. Butterworths; London: 1959.

52. DeCiantis CL, Jensen DK, Hudson BS, Borer PN. A nucleic acid switch triggered by the HIV-1 nucleocapsid protein. Biochemistry 2007;46:9164–9173. [PubMed: 17658889]

53. Deciantis, CL. PhD Dissertation. Syracuse University; 2008. A FRET Based Bistable Oligonucleotide Switch, AlloSwitch, Designed for Specific Recognition of HIV-1 NCp7 and Use in High Throughput Screening.

54. Wenner JR, Williams MC, Rouzina I, Bloomfield VA. Salt dependence of the elasticity and overstretching transition of single DNA molecules. Biophys J 2002;82:3160–3169. [PubMed: 12023240]

55. Paoletti, AC. PhD Dissertation. Syracuse University; 2004. Affinity of the HIV-1 nucleocapsid protein for structural motifs in the genomic RNA packaging domain.

56. Kaul M, Barbieri CM, Kerrigan JE, Pilch DS. Coupling of drug protonation to the specific binding of aminoglycosides to the A site of 16 S rRNA: elucidation of the number of drug amino groups involved and their identities. J Mol Biol 2003;326:1373–1387. [PubMed: 12595251]

57. Cruceanu M, Gorelick RJ, Musier-Forsyth K, Rouzina I, Williams MC. Rapid kinetics of protein-nucleic acid interaction is a major component of HIV-1 nucleocapsid protein's nucleic acid chaperone function. J Mol Biol 2006;363:867–877. [PubMed: 16997322]
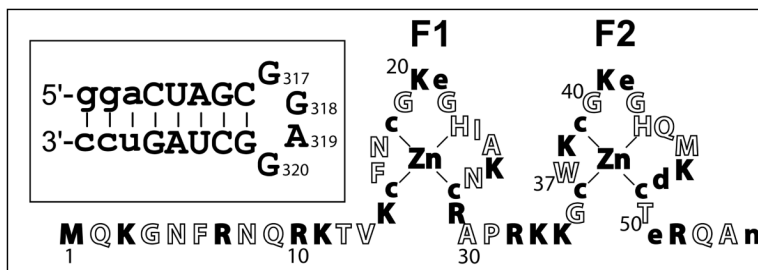
**Figure 1.**
The mature NCp7 protein from the pNL4-3 strain (wild-type I1 has been replaced with M1 for efficient expression in *E. coli*). Residues carrying a charge are shown in filled letters (positive = capitals, negative = lower-case); at neutral pH, NCp7 from pNL4-3 carries a +9 net charge = +1 (N-terminus), +15 (R, K side chains), −4 (D, E side chains), +4 (Zn²⁺), −6 (cysteine thiolates), −1 (C-terminus). The inset shows the SL3 sequence; residues in lower case are not present in wild-type SL3.
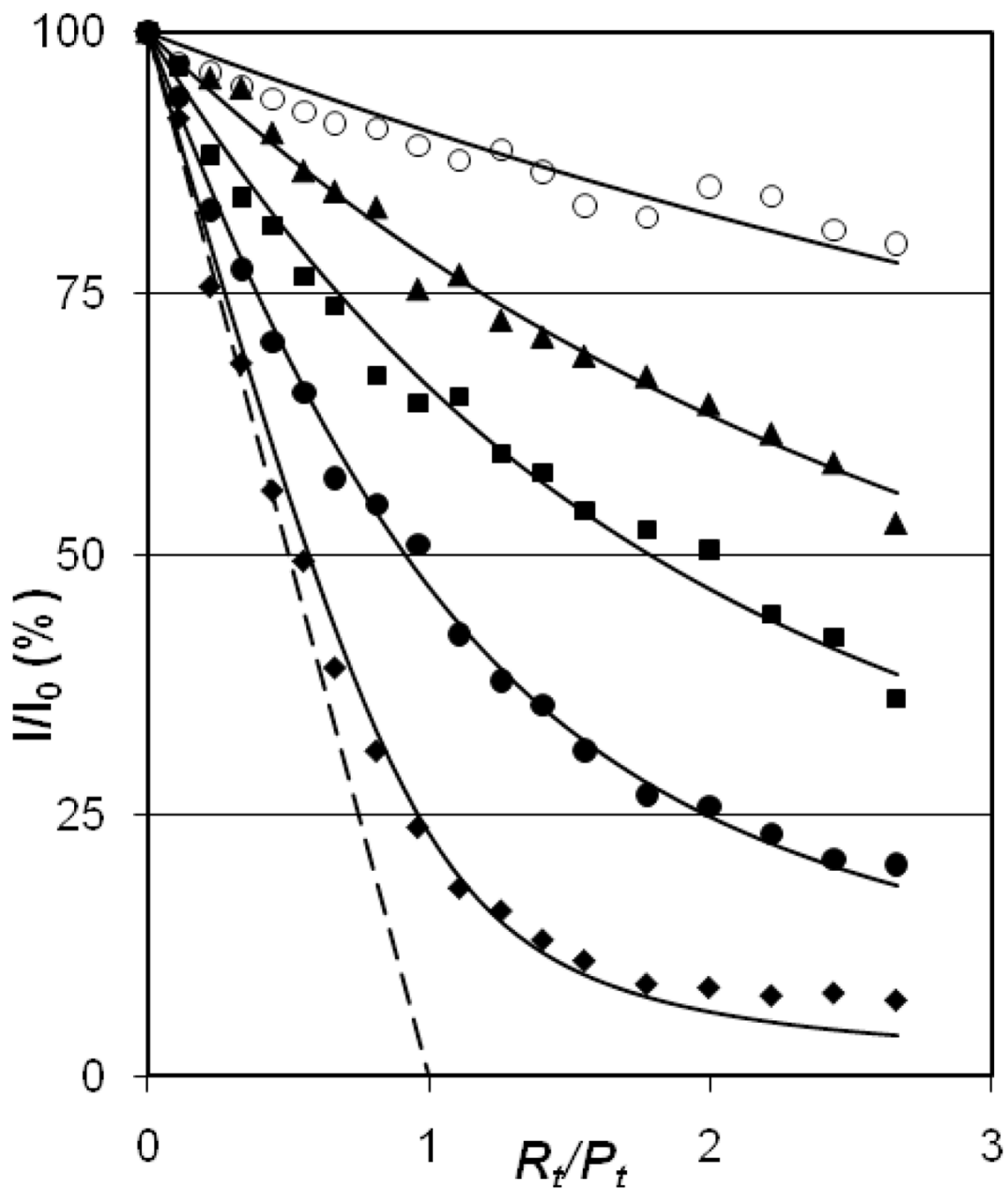
**Figure 2.**
Experimental AddNA assays where SL3 was added to NCp7. The binding isotherms are at progressively higher salt, bottom to top, with the long-dashed limit line representing infinitely high affinity for an $R_1P_1$ complex ($K_d \rightarrow 0$). Diamonds, 0.200 M NaCl (fitted with $K_d = 21$ nM); filled circles, 0.300 M ($K_d = 120$ nM); squares, 0.400 M ($K_d = 380$ nM); triangles, 0.500 M ($K_d = 840$ nM); open circles 0.800 M ($K_d = 2,600$ nM). The total protein concentration, $P_t = 0.30$ μM.
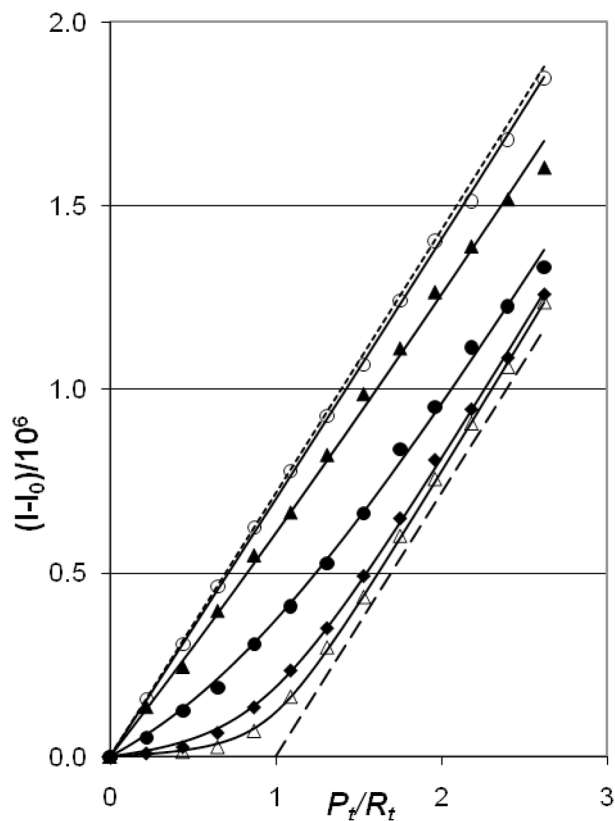
**Figure 3.**
Experimental AddPro assays where NCp7 was added to SL3 (total RNA concentration, $R_t$ = 0.30 μM). As in Fig. 2, isotherms at low salt appear near the bottom of the plot. I−$I_0$ is the difference between the measured fluorescence and the fluorescence at $P_t$ = 0. The symbols are defined as in Fig. 2 with the addition of open triangles, 0.150 M NaCl. Solid lines show isotherms fitted using $K_d$ = 9 nM for 0.150 M NaCl, $K_d$ = 25 nM for 0.200 M, $K_d$ = 140 nM for 0.300 M, $K_d$ = 1,120 nM for 0.500 M, 5,300 nM for 0.800 M. The limit lines represent $K_d \rightarrow 0$ (long dashes) and $K_d^{-1} \rightarrow 0$ (short dashes) for an $R_1P_1$ complex.
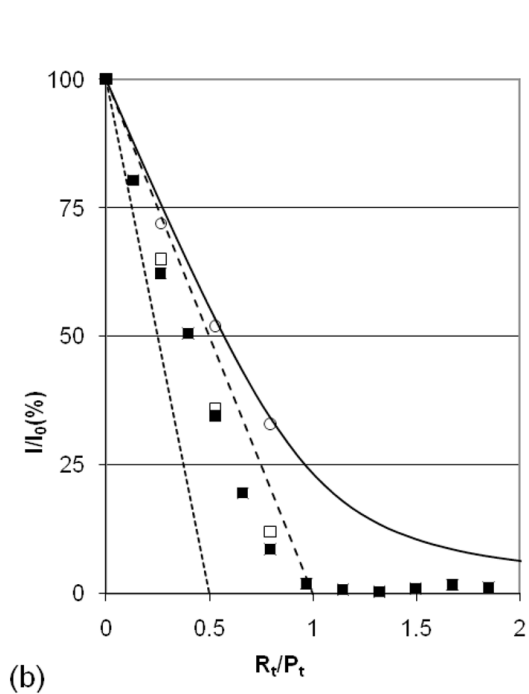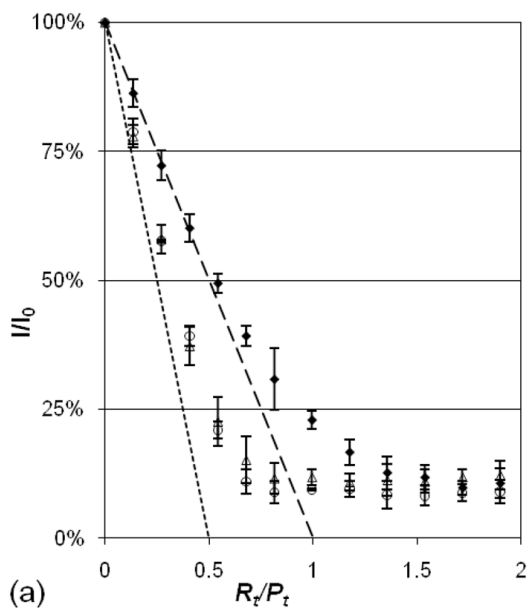
**Figure 4.**
AddNA assays at low [NaCl] measured as in Fig. 2. The limit lines are for $R_1P_1$ (long dashes) and $R_1P_2$ (short dashes; this line intersects the x-axis at the mole ratio, $R_t/P_t = 1/2$). Solid diamonds show 0.200 M NaCl data in both panels. (a) The error bars indicate one standard deviation about the average of three replicates; open triangles, 0.150 M NaCl, open circles, 0.100 M. (b) Filled squares show data for a full titration at 0.050 M NaCl. Open squares show the endpoints of three titrations with identical spacing of the earlier points. At each endpoint, salt was increased to [NaCl] = 0.200 M and fluorescence increased to the values indicated by open circles, which fall near the solid line calculated for $K_d = 21$ nM.
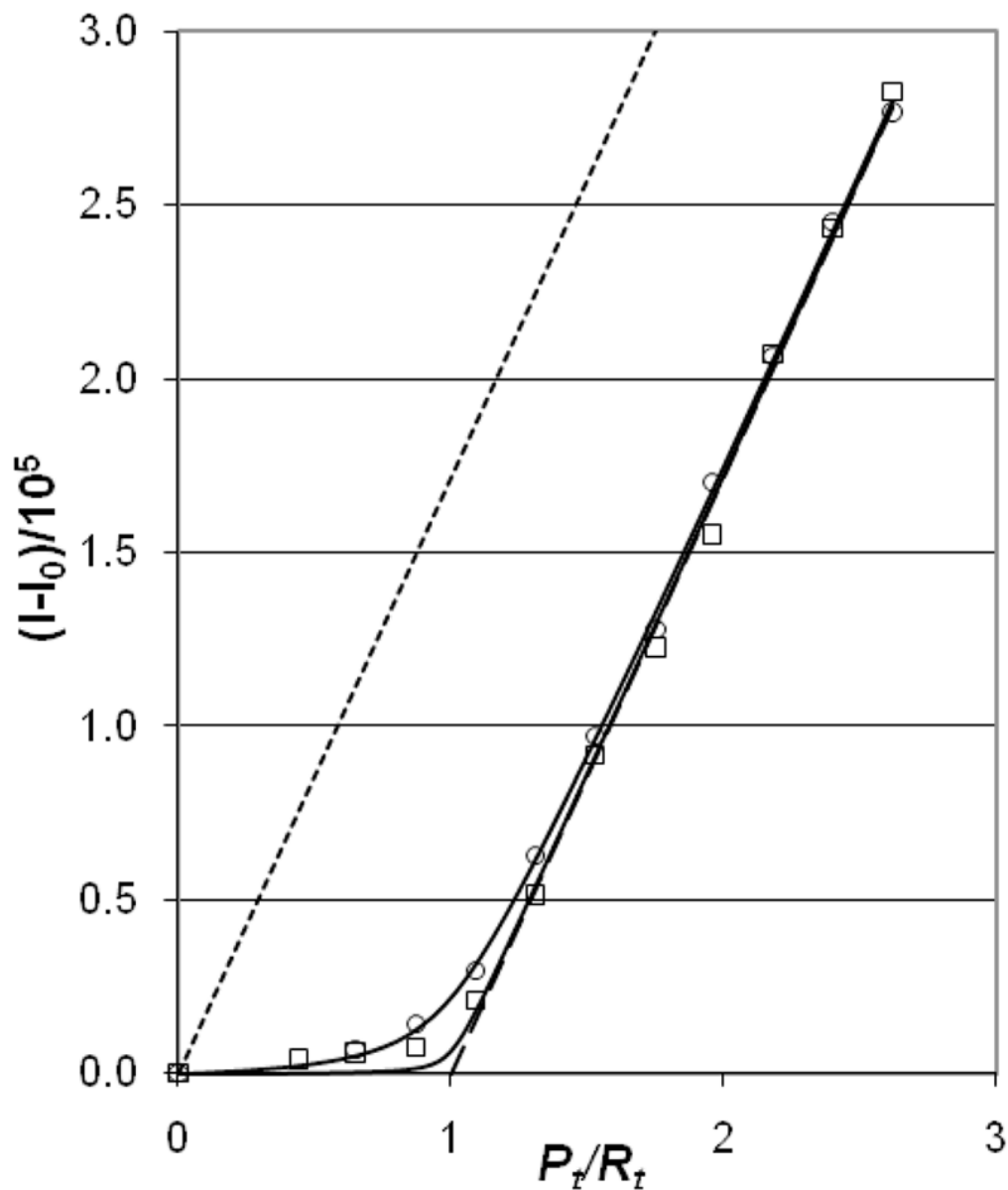
**Figure 5.**
AddPro assays for 0.100 M and 0.050 M [Na] at total RNA concentration, $R_t$ = 0.075 μM); solid lines show isotherms fitted to the data. Open circles, 0.100 M NaCl ($K_d$ = 1.4 nM), open squares, 0.050 M NaCl ($K_d$ = 0.3 nM). Limit lines are as in Fig. 3. The starting NCp7 and SL3 concentrations were diluted 4-fold from those shown in Fig. 3. Without this dilution, titrations for 0.100 and 0.050 M NaCl proceed along the x-axis to the breakpoint at $P_t/R_t$ = 1, and then follow the 1:1 line (data not shown).
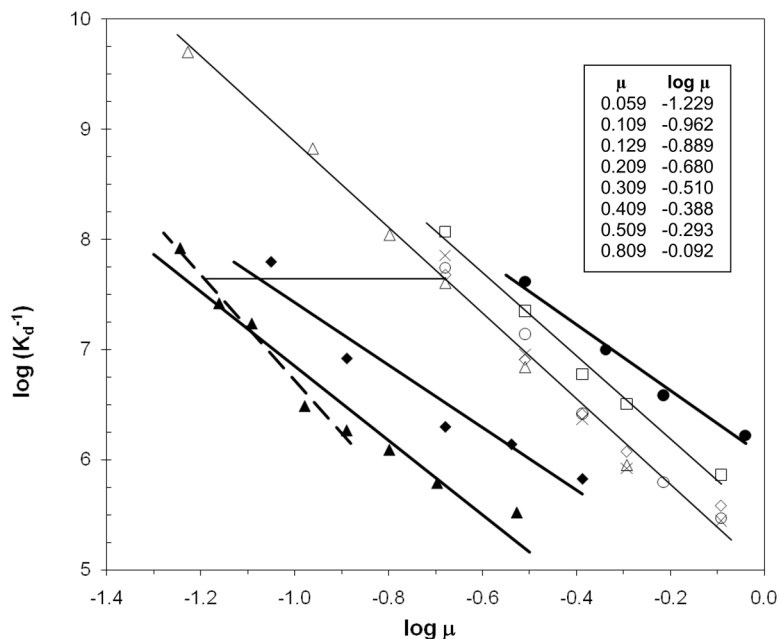
**Figure 6.**
Dependence of NCp7-SL3 binding on ionic strength for six salts. *Open symbols* and *light lines* are for salts with *monovalent ions*: sodium chloride (AddPro), triangles; (AddNA, this work), diamonds, (AddNA, previously reported (27)) circles; potassium chloride (AddNA, this work, ×); sodium acetate (AddNA), squares. Salts containing *divalent ions* are shown with *filled symbols* and *dark lines*: magnesium chloride (AddNA), triangles, (the shorter dashed line was fitted to points with $\mu \leq 0.129$ M); magnesium sulfate (AddNA), diamonds; sodium sulfate (Add NA), circles. Best-fit lines for the monovalent ions had the following slopes and standard errors: NaCl $-3.84 \pm 0.15$, KCl $-4.16 \pm 0.42$ (line not shown), NaOAc $-3.77 \pm 0.22$. The thin horizontal line links the $MgCl_2$ and NaCl lines where both have $K_d = 23$ nM (at [NaCl] = 0.20 M, [$MgCl_2$] = 0.018 M). The nomogram (upper right) helps to interpret the x-axis. It includes several $\mu$ values used in the experiments and their corresponding logarithms ($\mu$ includes the 0.009 M contribution from the invariant buffer components (sodium phosphate, zinc chloride)).

**Table 1**

$K_d$ values[*] upon varying [NaCl].

| NaCl] (M) | N | $K_d$(av) (nM) | $K_d$(slope) (nM) |
|-----------|---|----------------|-------------------|
| 0.800 | 2 | 3800 | 4400 |
| 0.500 | 2 | 980 | 730 |
| 0.400 | 2 | 380 | 310 |
| 0.300 | 3 | 110 ±40 | 110 |
| 0.200 | 38 | 21 ±2 | 23 |
| 0.100 | 5 | 1.5 ±0.6 | 1.9 |
| 0.050 | 2 | 0.2 | 0.18 |
| 0.010 | -- | -- | 0.022 |

[*] Dissociation constants, $K_d$(av), are averages of values of individual determinations at the indicated [NaCl] for the NCp7-SL3 complex, (standard deviations are shown for determinations with ≥3 replicates). The number of replicates is N; $K_d$(slope) was predicted from the plot in Figure 6. Trailing zeroes in $K_d$ values are not significant digits. $K_d$ values at [NaCl] < 0.200 M are from AddPro assays, whereas values at [NaCl] > 0.300 M are from AddNA data. $K_d$ values averaged in Table 1 for 0.100 and 0.050M NaCl are from AddPro measurements at $R_t$ = 0.075 μM. In addition to the indicated [NaCl] the buffer components add 0.0091 M to the ionic strength (see Experimental).